# Arbitrary Shaped Objects Detection and Reconstruction through Overset Grid Generation Method with $B_2$-spline Interpolation in Forward-Backward Time-Stepping Inverse Scattering

**Bong S. Wee [1, 2], Kismet A. H. Ping [1], Shafrida Sahrani [1], and Toshifumi Moriyama [3]**

[1] Applied Electromagnetic Research Group, Department of Electrical and Electronic Engineering
Faculty of Engineering, Universiti Malaysia Sarawak, Kota Samarahan, 94300, Malaysia
bongsw@pmu.edu.my, hpkismet@unimas.my, sshafrida@unimas.my

[2] Department of Electrical Engineering
Politeknik Mukah, Mukah, 96400, Malaysia
bongsw@pmu.edu.my

[3] Department of Electrical and Electronic Engineering, Graduate School of Engineering
Nagasaki University 1-14 Bunkyo-machi, Nagasaki, 852-8521, Japan
t-moriya@nagasaki-u.ac.jp

***Abstract*** ─ Finite-Difference Time-Domain (FDTD) method is a simple and powerful tool used to solve electromagnetic (EM) problems. However, the drawbacks of FDTD method are difficult to model the curved boundaries and small features due to its restriction to inherent orthogonal grids. We have previously proposed that the $B_2$-spline or biquadratic spline interpolation technique for Overset Grid Generation and Finite-Difference Time-Domain (OGG-FDTD) method be utilised to overcome the limitations of FDTD method. This proposed method has the ability to accurately measure a scattered field around an unknown object. In this paper, the OGG-FDTD method with $B_2$-spline interpolation in Forward-Backward Time-Stepping (FBTS) inverse scattering technique was proposed for the detection and reconstruction of arbitrary shaped objects in Case A and malignant breast tumour detection in Case B. The results showed that the Mean Square Error (MSE) of reconstructed dielectric profiles by using the proposed method has achieved significantly lower values than the FDTD method in FBTS. In Case A, the accuracy difference between the two methods was 26.67% for relative permittivity and 27.63% for conductivity, respectively. In Case B, it was found that the implementation of the proposed method increased the accuracy of reconstructed the relative permittivity image by 50.54%, and conductivity by 74.42% as compared to the FDTD method in FBTS technique. Furthermore, the values of normalised error function for the proposed method were also lower than the FDTD method in FBTS. Hence, it is proven that this numerical method can provide clearer and better reconstructed images to improve the quality of retrieve the dielectric profiles of the investigation area.

***Index Terms*** ─ $B_2$-spline interpolation, buried object detection, inverse scattering problem, overset grid generation method.

## I. INTRODUCTION

Microwave tomography is the new technology which evaluates buried or embedded objects in a medium by using EM waves. The main applications of microwave tomography are ground-penetrating radar [1-3], buried object detection applications in remote sensing [4-6], non-destructive evaluation [7-9], and medical diagnostic for biomedical engineering [10-13]. Microwave imaging technique (MWT) for non-destructive evaluation utilises frequency-domain [14] or time-domain [15] to solve the electromagnetic (EM) scattering problems. The EM scattering problems can be classified into two, which are direct and inverse scattering problems, respectively. The inverse scattering problem is the problem of determining characteristics of an unknown objects from the measurement data of a scattered field based on the actual objects detected [16].

Several methods have been reported in literature for solving the inverse scattering problem such as Bojarski-Lewis method [17], Linear Sampling method [18], and Lagrange Multipliers method [19]. However, those methods have some limitations such as instability, fails to estimate the target support for certain frequencies, and needed a large number of data for images reconstruction. Therefore, the Forward-Backward Time-Stepping (FBTS)

*Submitted On: February 7, 2019*
*Accepted On: October 23, 2019*

1054-4887 © ACES

inverse scattering technique by Takenaka et al. [20] is utilised in this paper. The FBTS technique (also known as an iterative inversion technique) can be used to obtain the unknown electrical properties of objects by inverting measure scattered-field data. Furthermore, the useful quantitative information of the objects (e.g., its shapes, dimensions, locations and dielectric properties) also can be determined by utilising FBTS technique.

Finite-Difference Time-Domain (FDTD) method is a simple and powerful tool by which to solve Electromagnetic (EM) problems such as scattering from metal objects and dielectrics, microstrip circuits, antenna analysis, electromagnetic wave propagation, and human exposure to EM waves [21, 22]. It can investigate multiple frequencies without any extra computational effort. However, the limitations of the FDTD method are difficult to model the curved boundaries and small features due to its restriction to inherent orthogonal grids [23, 24]. Several methods have been reported in literature to improve the efficiency of the FDTD method, such as sub-gridding, non-uniform, and sub-cell algorithm [25-27]. However, those methods still have some drawbacks such as: requiring high computation time and more memory; as well as time step or cell size being restrictive by the Courant-Friedrichs-Lewy (CFL) stability condition [28]. Previously, we proposed the $B_2$-spline interpolation technique for Overset Grid Generation and Finite-Difference Time-Domain (OGG-FDTD) method to overcome these limitations [29]. This method has the ability to accurately measure the EM scattered field for an unknown object in a different medium.

In this paper, the OGG-FDTD method with $B_2$-spline interpolation in Forward-Backward Time-Stepping (FBTS) inverse scattering technique is proposed for the detection and reconstruction of arbitrary shaped objects and realistic breast composition. The performance of the proposed method is evaluated by investigating the characteristics of arbitrary shaped objects in transverse magnetic $z$-plane ($TM_z$) mode. The conjugate gradient minimisation method by Fletcher-Reeves and Polak-Ribiere-Polyak was used in this work for optimisation technique in order to reconstruct the microwave images.

## II. OVERSET GRID GENERATION METHOD WITH $B_2$-SPLINE INTERPOLATION IN FORWARD-BACKWARD TIME-STEPPING INVERSE SCATTERING TECHNIQUE

Figure 1 (a) shows the actual image of two homogenous arbitrary shaped objects. These objects are embedded in the Region of Interest (ROI) with free space as the background medium. Figure 1 (b) shows the reconstructed image by utilising the OGG-FDTD method with $B_2$-spline interpolation in FBTS inverse scattering technique. The OGG-FDTD lattice consists of two meshes, namely, main-mesh and sub-mesh. The sub-mesh was set to overlap on top and centre of the main mesh and used to model the arbitrary shaped objects.

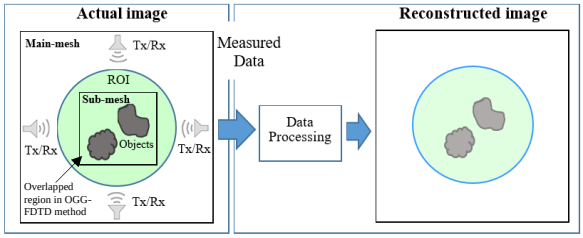


Fig. 1. Configuration of OGG-FDTD method with $B_2$-spline interpolation in FBTS inverse scattering technique. 'Tx/Rx' indicates the transmission and receiving antennas.

The FBTS technique can be separated into two steps: forward step and backward step [20]. The forward step of the FBTS method begins with the excitation of Gaussian pulse signal to the estimated profile of the arbitrary shaped objects. The OGG-FDTD method with $B_2$-spline interpolation was used to calculate the scattered fields for forward time-stepping. The $B_2$-spline interpolation was used to interpolate the EM field for the overlapped region in OGG-FDTD lattice as shown in Fig. 2. $B_2$-spline interpolation is using a set of lower order polynomials between known values data points at main mesh to determine the unknown value data point at sub-mesh.

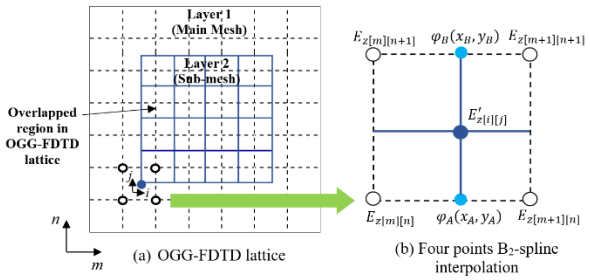


Fig. 2. The overlapped region in OGG-FDTD method with $B_2$-spline interpolation.

The EM field components on the main mesh are set as $E_z$, $H_x$, and $H_y$ while on the sub-mesh are set as $E'_z$, $H'_x$ and $H'_y$. The electric field on main mesh ($E_z$) is interpolated to sub-mesh ($E'_z$) through $B_2$-spline interpolation technique. $Ez_{[m][n]}(x_1, y_1)$, $Ez_{[m+1][n]}(x_2, y_2)$, $Ez_{[m][n+1]}(x_3, y_3)$, and $Ez_{[m+1][n+1]}(x_4, y_4)$ are the four known value points at the main-mesh, while $E'_{z_{[i][j]}}(x_s, y_s)$ is the unknown value point at the sub-mesh. Where, $m$ and $n$ are the number of cell grids for main-mesh, whereas $i$ and $j$ are the number of cell grids for sub-mesh. The

unknown value of $\varphi_A(x_A, y_A)$ is interpolated by using the known values of $Ez_{[m][n]}(x_1, y_1)$ and $Ez_{[m+1][n]}(x_2, y_2)$ whereas the unknown value of $\varphi_B(x_B, y_B)$ is interpolated by using the known values of $Ez_{[m][n+1]}(x_3, y_3)$ and $Ez_{[m+1][n+1]}(x_4, y_4)$ at the $x$-axis. Then, the unknown value of $E'_{Z_{[i][j]}}$ can be calculated by using the $\varphi_A$ and $\varphi_B$ at $y$-axis as follows:

$$E'_{Z_{[i][j]}} = \left[\frac{d_{y1_{[m][n+1]}} - d_{y1_{[m][n]}}}{2(y_B - y_A)}\right](y_s - y_A)^2 + \left[d_{y_{[m][n]}}\right](y_s - y_A) + \varphi_A, \quad (1)$$

$$i = 0,1,2, \ldots \text{ and } j = 0,1,2 \ldots$$

where,

$$d_{y1_{[m][n]}} = 0,\ d_{y1_{[m][n+1]}} = \frac{2(\varphi_B - \varphi_A)}{(y_B - y_A)} - d_{y1_{[m][n]}},$$

$$\varphi_A = \left[\frac{d_{x1_{[m][n+1]}} - d_{x1_{[m][n]}}}{2(x_2 - x_1)}\right](x_A - x_1)^2 + \left[d_{x1_{[m][n]}}\right](x_A - x_1) + E_{Z_{[m][n]}},$$

$$\because d_{x1_{[m][n]}} = 0,\ d_{x1_{[m][n+1]}} = \frac{2\left(E_{Z_{[m+1][n]}} - E_{Z_{[m][n]}}\right)}{(x_2 - x_1)} - d_{x1_{[m][n]}},$$

$$\varphi_B = \left[\frac{d_{x2_{[m][n+1]}} - d_{x2_{[m][n]}}}{2(x_4 - x_3)}\right](x_B - x_3)^2 + \left[d_{x2_{[m][n]}}\right](x_B - x_3) + E_{Z_{[m][n+1]}},$$

$$\because d_{x2_{[m][n]}} = 0, d_{x2_{[m][n+1]}} = \frac{2\left(E_{Z_{[m+1][n+1]}} - E_{Z_{[m][n+1]}}\right)}{(x_4 - x_3)} - d_{x2_{[m][n]}},$$

$$m = 0,1,2, \ldots \text{ and } n = 0,1,2 \ldots .$$

Similarly, the $H_x$ and $H_y$ fields for the overlapped region in OGG-FDTD lattice were interpolated by using the same interpolation process.

Then, the $E_z'$ fields on the sub-mesh were interpolation back into the main mesh, so that the electric fields ($E_z$) on the main mesh are updated. This algorithm continued until the time-stepping was concluded. The details regarding OGG-FDTD method with $B_2$-spline interpolation can be found in [29].

The forward time-stepping reconstructions data at the receiving point were collected and compared with the measurement data. The backward step of the FBTS method was used to calculate the adjoint field in OGG-FDTD lattice. The adjoint field is the field which radiates from the equivalent impressed currents of the different of the forward time-stepping reconstructions data and measurement data. Then, the backward time-stepping reconstructions data at the receiving point were collected and compared with the measurement data. The difference between measured and calculated scattered fields was utilised as a source by which to irradiate the original profile.

The cost functional, $Q(p)$ was used to minimise the number of iterations for the FBTS reconstruction as shown in (2):

$$Q(p) = \int_0^T \sum_{m=1}^{M} \sum_{n=1}^{N} K_{mn}(t)\ |V_m(p; r_n^r, t) - \tilde{V}_m(r_n^r, t)|^2 dt, \quad (2)$$

where, $K_{mn}(t)$ is a non-negative weighting function, and $T$ is the time duration of measurement. $V_m(r_n, t)$ is the calculated electromagnetic fields vector for an estimate's medium parameter vector $p$, and $\tilde{V}_m(r_n, t)$ is the measured EM fields vector for the $m^{\text{th}}$ source. The cost functional was computed by comparing the estimated profiles to the actual profiles until the different between both profiles are lower.

Following this, the estimated permittivity values for the next iteration are as shown in (3):

$$\varepsilon_r^{k+1}(r) = \varepsilon_r^k(r) + \alpha^k d_\varepsilon^k(r), \quad (3)$$

where, $k$ is the current optimisation iteration number in the FBTS optimisation, $\varepsilon_r^k(r)$ indicates permittivity values in the reconstruction region, $d_\varepsilon^k(r)$ is search direction, $r$ represents variation in space (i.e., $r$ gives the $x$, $y$ spatial coordinate), and $\alpha^k$ is the approximate step-size.

An analytical approximation approach is used to calculate the step size, $\alpha$ by substituting the term $p = \varepsilon_r + \alpha d_\varepsilon$ from (3) into (2). The cost functional, $Q(p)$ for current iteration can be calculated as follows:

$$Q(p) = \int_0^T \sum_{m=1}^{M} \sum_{n=1}^{N} K_{mn}\ |v_m(\varepsilon_r + \alpha d_\varepsilon) - \tilde{v}_m|^2 dt. \quad (4)$$

Then, calculate the cost functional $Q(p)$for the 1st iteration as reference:

$$Q_{Vm}(p) = \int_0^T \sum_{m=1}^{M} \sum_{n=1}^{N} K_{mn} |\tilde{v}_m|^2\, dt. \quad (5)$$

The normalisation of $Q(p)$ can be calculated by utilizing (4) and (5) as:

$$\text{Normalisation of } Q(p) = \frac{Q(p)}{Q_{Vm}(p)}. \quad (6)$$

The conjugate gradient minimisation methods by Fletcher-Reeves and Polak-Ribiere-Polyak were used as optimisation techniques for optimal control of machine computation problems and also to minimise the functional error. The gradient functional can be obtained by introducing the Fréchet derivative to (2). The gradient vectors are then found with respect to the permittivity and conductivity as demonstrated in (7) and (8).

$$g_{\varepsilon_r}(r) = \int_0^T \sum_{m=1}^{M} \sum_{i=1}^{2} w_{mi}\begin{pmatrix} p; \\ r, \\ t \end{pmatrix} \frac{\partial}{\partial(t)}\ v_{mi}\begin{pmatrix} p; \\ \mathrm{r}, \\ t \end{pmatrix} dt, \quad (7)$$

$$g_\sigma(r) = \int_0^T \sum_{m=1}^{M} \sum_{i=1}^{2} w_{mi}(p; r, t) v_{mi}(p; \mathrm{r}, t) d\mathrm{t}. \quad (8)$$

The terms $v_{mi}(p; r, t)$ and $w_{mi}(p; r, t)$ refer as the $i^{\text{th}}$ component of the EM field, $v_m(p; r, t)$ and adjoint field vector, $w_m(p; r, t)$. The adjoint fields are calculated by propagating the residual scattered signals being reversed in time and utilised as sources. The summation term from $i = 1$ to $i = 2$ represents the fact that in two-dimensional (2D) the gradients are calculated using the $x$- and $y$-components of $v_{mi}$ and $w_{mi}$.

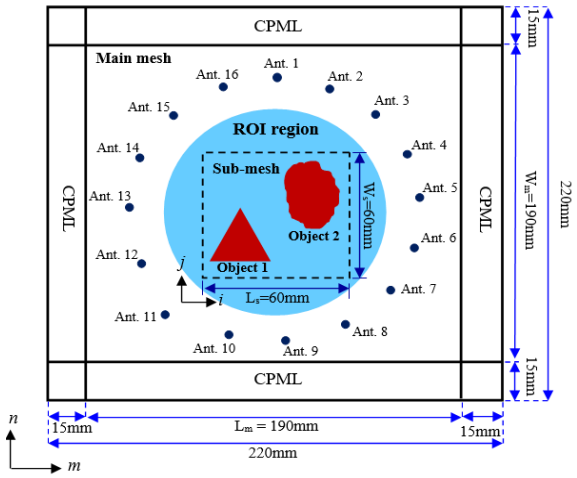


Fig. 2. Configuration of arbitrary shaped objects in 2D OGG-FDTD scheme.

## III. NUMERICAL MODEL SETUP

Figure 2 shows the configuration of an active microwave tomography in 2D. The OGG-FDTD method with $B_2$-spline interpolation in FBTS technique was used to solve the non-dispersive inverse scattering problem in $TM_Z$. The actual dielectric profiles setting is listed as in Table 1.

Table 1: Actual dielectric profiles setting

| Layer | Media Region | $\varepsilon_r$ (F/m) | σ (S/m) |
|---|---|---|---|
| Layer 1 (Main-mesh) | Background | 1.00 | 0.00 |
| | ROI | 9.98 | 0.18 |
| Layer 2 (Sub-mesh) | Arbitrary shaped objects | 21.45 | 0.46 |

The main-mesh was set to 190 mm × 190 mm grids and the sub-mesh was set to 60 mm × 60 mm grids. The Region of Interest (ROI) is a circular shape with a radius of 50 mm and located on the middle of the main-mesh. The dielectric properties of the ROI are assumed to be the fatty tissues, and the arbitrary shaped objects are assumed to be the fibroglandular tissues in the breast. The background of the FDTD lattice is assumed to be free space. Reconstructions were conducted by utilising the 1 mm × 1 mm OGG-FDTD grid size and the optimisation was carried out for 100 iterations. A sinusoidal modulated Gaussian pulse with centre frequency of 2.0 GHz and bandwidth of 1.3 GHz acted as the excitation signal in the simulations. Sixteen (16) points represented as antennas encircle the ROI with a radius of 85 mm. Each of the point source antennas acted as a transmitter that sequentially transmitted a Gaussian pulse. The remaining 15 antennas became the receivers to collect the scattered fields in the OGG-FDTD lattice. The details regarding the effect of different MWT parameters such as the noise of the scattered data, number of antennas, and frequency of operation can be found in [11, 30, 31]. The Convolution Perfectly Matched Layer (CPML) with 15 cells are utilised in this work as absorbing boundary condition (ABC) to absorb the travelling wave without reflections from the edge.

## IV. RESULTS AND DISCUSSION

In this section, the performance of OGG-FDTD method with $B_2$-spline interpolation in Forward-Backward Time Stepping (FBTS) inverse scattering for the detection and reconstruction of buried objects is being evaluated. A homogenous arbitrary shaped object is chosen in this research to validate the competency of the proposed method in Case 1. Then, the efficacy of this proposed method is applied to inhomogeneous realistic breast cancer detection application in Case 2.

### A. Case 1: Multiple arbitrary shaped objects

Figure 3 illustrates the actual and reconstructed relative permittivity profiles of the numerical model in Case 1. The actual profile of the relative permittivity is presented in Fig. 3 (a), whereas the reconstructed relative permittivity images are shown in Figure 3(b) for FDTD method in FBTS, and Fig. 3 (c) for OGG-FDTD method with $B_2$-spline interpolation in FBTS. The curved boundaries and small features of an arbitrary shaped objects cannot be modelled by using the FDTD method in FBTS. In contrast, the OGG-FDTD method with $B_2$-spline interpolation in FBTS is able to accurately reconstruct the curved boundaries and small features of an arbitrary shaped objects.

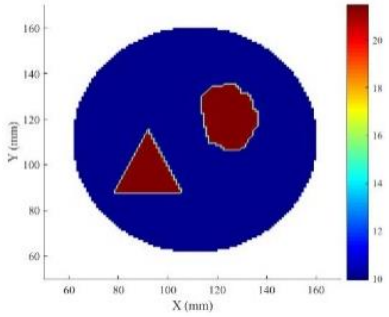


(a) Actual relative permittivity

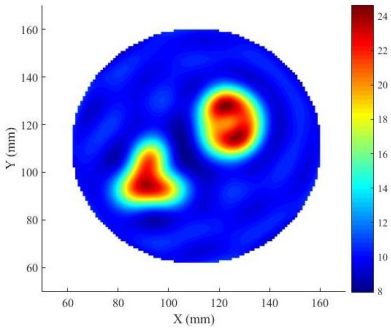


(b) Reconstructed relative permittivity profile for FDTD method in FBTS

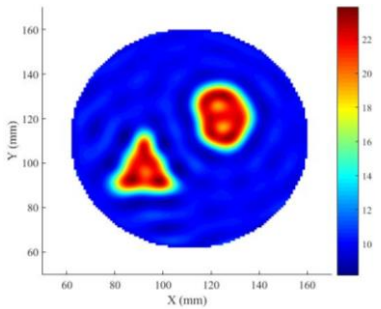


(c) Reconstructed relative permittivity profile for OGG-FDTD method with $B_2$-spline interpolation in FBTS

Fig. 3. Actual and reconstructed relative permittivity profiles of the arbitrary shaped objects in Case 1.

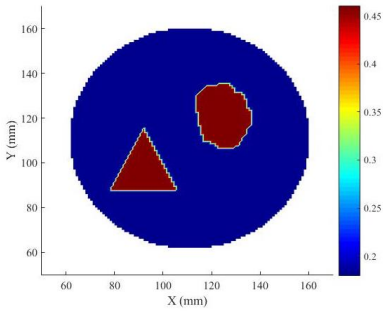


(a) Actual conductivity

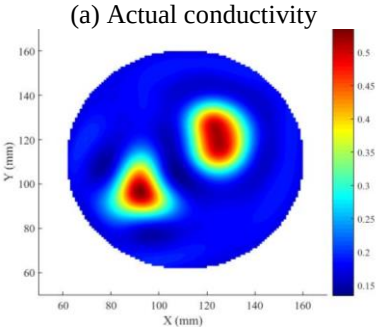


(b) Reconstructed conductivity profile for FDTD method in FBTS

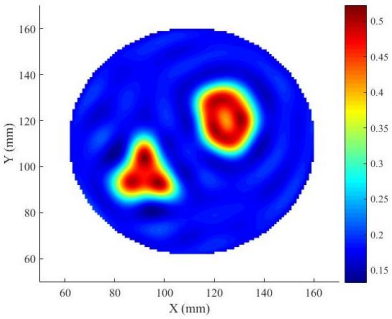


(c) Reconstructed conductivity profile for OGG-FDTD method with $B_2$-spline interpolation in FBTS

Fig. 4. Actual and reconstructed conductivity profiles of the arbitrary shaped objects in Case 1.

Figure 4 illustrates the actual and reconstructed conductivity profiles of the numerical model in Case 1. Figure 4 (a) depicts the original profile of the conductivity, whereas Fig. 4 (b) shows the reconstructed conductivity image for FDTD method in FBTS, and Fig. 4 (c) shows the reconstructed conductivity image for OGG-FDTD method with $B_2$-spline interpolation in FBTS. The OGG-FDTD method with $B_2$-spline interpolation in FBTS inverse scattering technique was successfully detected and accurately reconstructed the conductivity profiles of arbitrary shaped objects. The accuracy of the OGG-FDTD method with $B_2$-spline interpolation in FBTS was investigated by using the Mean Square Error (MSE) as follows:

$$\text{MSE} = \frac{\sum_{M,N}[P_A(x,y)-P_R(x,y)]^2}{MN}, \quad (9)$$

where, $P_A(x,y)$ is actual dielectric profile, $P_R(x,y)$ is reconstructed profile, and $M \times N$ is an image's dimension. Table 2 shows the MSE analysis for these two methods. The results showed that MSE of reconstructed dielectric profiles by using the proposed method has achieved significantly lower values than the FDTD method in FBTS. The accuracy difference between the two methods was 26.65% for relative permittivity profile and 27.63% for conductivity profile. It has been proven that the OGG-FDTD method with $B_2$-spline interpolation in FBTS inverse scattering technique can provide accurate results and further improve the quality of reconstructed images such as its location, shape, size and internal composition, respectively.

Table 2: MSE of dielectric profiles

| **Methods** | **MSE** | |
|---|---|---|
| | **Relative Permittivity Profile** | **Conductivity Profile** |
| FDTD method in FBTS | 2.064 | $1.52 \times 10^{-3}$ |
| OGG-FDTD method with $B_2$-spline interpolation in FBTS | 1.514 | $1.10 \times 10^{-3}$ |

The accuracy of the OGG-FDTD method with $B_2$-spline interpolation in FBTS inverse scattering technique was further investigated by normalising the functional error. Figure 5 shows the normalised functional error versus the number of iterations. It was found that the normalised functional error decreased when the number of iterations increased. As can be seen, the normalised functional error for the OGG-FDTD method with $B_2$-spline interpolation in FBTS is lower as compared to the FDTD method. At the $100^{\text{th}}$ iteration, the difference of normalised functional error between these two methods was $6.06 \times 10^{-8}$. Hence, the OGG-FDTD method with $B_2$-spline interpolation in FBTS has the ability to retrieve the dielectric profiles accurately.

**B. Case 2: Heterogeneous dense realistic breast**

The mammograms for four breast parenchymal density based on BI-RADS [32] are: Class A (mostly fatty breast); Class B (scattered density breast); Class C (heterogeneously dense breast); and Class D (extremely dense breast). In order to analyse the accuracy of the OGG-FDTD method with $B_2$-spline interpolation in FBTS inverse scattering technique to detect a malignancy tumour embedded in arbitrary shaped of the fibroglandular region, the heterogeneous dense realistic breast was described in Case 2.

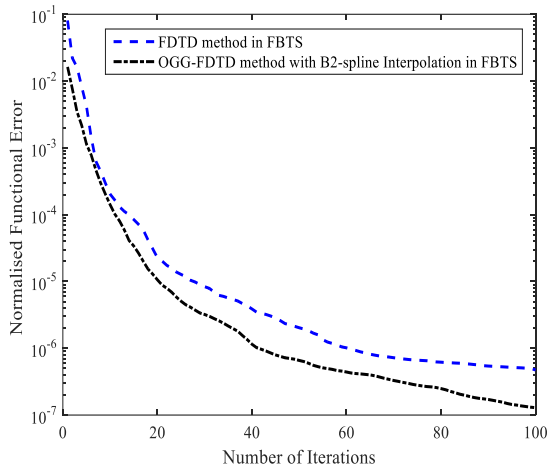


Fig. 5. Normalised functional error versus number of iterations.

The heterogeneously dense breast (also known as Class C breast) has large areas of dense fibrous and glandular breast tissue. Hence, it is difficulties to spot abnormalities in the Class C than in Classes A, and B, respectively. The heterogeneously dense breast phantom from Nagasaki University Hospital was chosen in this research for inhomogeneous breast cancer detection application. The breast tissues in this phantom have realistic ultra-wideband dielectric properties and can be readily used in FDTD computational electromagnetic models. This phantom is derived from a series of T1-weighted magnetic resonance images (MRIs) of patients in a prone position. Each numerical phantom comprised a three-dimensional (3D) grid of cubic voxels, where each voxel measures 0.5 mm × 0.5 mm × 0.5 mm. This 3D anatomical model was transformed into non-dispersive dielectric properties utilising spatial distributions. In order to satisfy the OGG-FDTD grid size, this model needed to resize from 0.5 mm × 0.5 mm × 0.5 mm to 1.0 mm × 1.0 mm × 1.0 mm. The resize process was implemented by using linear interpolation technique. Figure 6 illustrates the 2D numerical setup of an active microwave tomography for breast in OGG-FDTD lattice.

In this research, the non-dispersive heterogeneously dense breast composition was assumed to be immersed in a free space as a background medium. The FDTD lattice as main mesh is consists of 190 mm × 190 mm cells and surrounded by fifteen-cell of Convolution Perfectly Matched Layer (CPML). The sub-mesh is overlapping on top of the main mesh with 90 mm × 130 mm cells. The cell size for main-mesh and sub-mesh is $\Delta x = 1$ mm and $\Delta y = 1$ mm. The sub-mesh was modelled as an entire numerical breast phantom. A radius of 5 mm tumour was added in the fibroglandular region of the numerical breast. The actual setting of numerical measured data is referring to nominal Debye parameters as shown in Table 3. Skin, adipose, fibroglandular, and tumour are the four kinds of breast tissues.

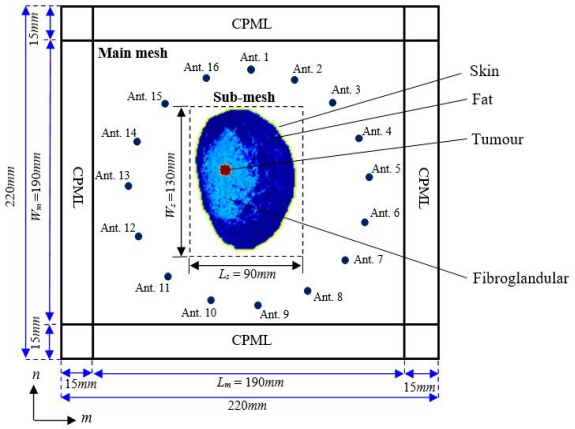


Fig. 6. Configuration of the realistic breast phantom in 2D view.

Table 3: Electronic property parameters utilised for breast tissue [20]

| Tissue | $\varepsilon_r$ (2 GHz) | σ (2 GHz) |
|---|---|---|
| Skin | 36.73 | 0.46 |
| Adipose | 9.98 | 0.18 |
| Fibroglandular | 21.45 | 1.43 |
| Tumour | 53.62 | 1.19 |

The sinusoidal modulated Gaussian pulse is used as excitation signal with centre frequency of 2.0 GHz and a bandwidth of 1.3 GHz. The OGG-FDTD method with biquadratic spline interpolation in FBTS inverse scattering technique was simulated up to 150 iterations to reconstruct the image of internal breast composition.

Figure 7 (a) shows the actual relative permittivity profile of non-dispersive heterogeneous dense realistic breast. Figure 7 (b) illustrates the reconstructed relative permittivity profile of the FDTD method in FBTS. Figure 7 (c) shows reconstructed relative permittivity profile of the OGG-FDTD method with $B_2$-spline interpolation in FBTS. These two methods have successfully reconstructed the malignancy tumour placed within the fibroglandular region. However, the reconstructed images

by these two methods are slightly different as compared to the actual distribution image. The curved boundaries and small features of an arbitrary shaped fibroglandular region cannot be modelled by using the FDTD method in FBTS. In contrast, the OGG-FDTD method with $B_2$-spline interpolation in FBTS was able to accurately reconstruct the curved boundaries and small features of an arbitrary shaped of the fibroglandular region.

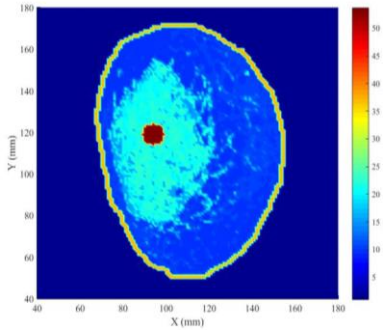


(a) Actual relative permittivity profile

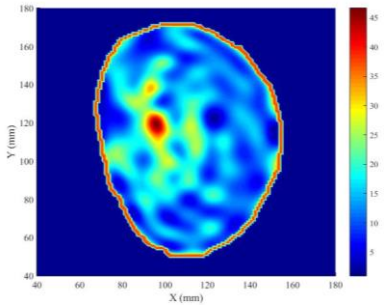


(b) Reconstructed relative permittivity profile for FDTD method in FBTS

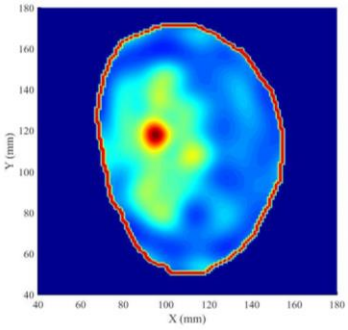


(c) Reconstructed relative permittivity profile for OGG-FDTD method with $B_2$-spline interpolation in FBTS

Fig. 7. Actual and reconstructed relative permittivity profiles of the breast phantom in Case 2.

Figure 8 (a) shows the actual conductivity profile of a heterogeneous dense realistic breast phantom in Case 2. As illustrated in Fig. 8 (b), the embedded tumour is unable to be detected in conductivity reconstruction by utilising the FDTD method in FBTS. To address this issue, a new numerical method based on the OGG-FDTD method with $B_2$-spline interpolation in FBTS inverse scattering technique was proposed to determine the presence and location of malignant tumours in the breast. Whereas, the proposed method has successfully detected and reconstructed the breast composition of the conductivity profile as depicted in Fig. 8 (c). Reconstructed image clearly indicates the value of the dielectric parameters as being almost identical to the true values of the tumour located within the fibroglandular region as well as its position and size.

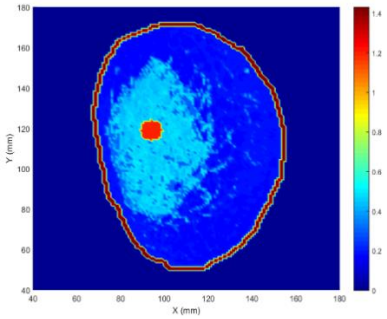


(a) Actual conductivity profile

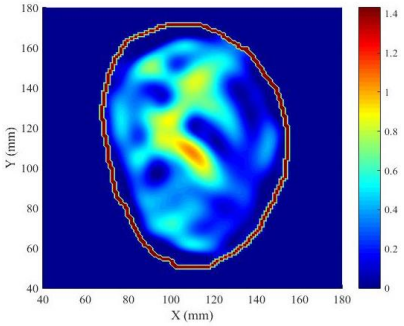


(b) Reconstructed conductivity profile for FDTD method in FBTS

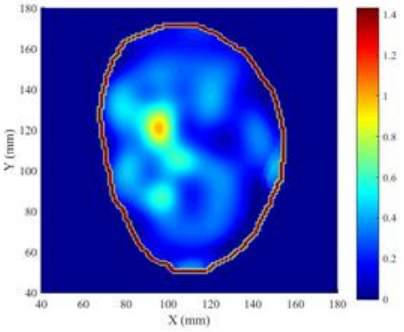


(c) Reconstructed conductivity profile for OGG-FDTD method with biquadratic spline interpolation in FBTS

Fig. 8. Actual and reconstructed conductivity profiles of the breast phantom in Case 2.

The accuracy of actual and reconstructed profiles can be investigated by using Mean Square Error (MSE). In terms of MSE level, the reconstructed relative permittivity profile by the FDTD method in FBTS

attained an accuracy of rating 24.829 while the OGG-FDTD method with $B_2$-spline interpolation in FBTS attained an accuracy level of 12.279. It was found that the implementation of the OGG-FDTD method in FBTS technique increased the accuracy of reconstructed the relative permittivity image by 50.54% as compared to the FDTD method in FBTS technique. Further, the MSE for reconstructed conductivity profile achieved an accuracy level of 0.043 for the FDTD method in FBTS, while the OGG-FDTD method in FBTS achieved an accuracy rating of 0.011. Hence, the MSE for reconstructed conductivity profile utilising the proposed method achieved significantly lower values than the FDTD method in FBTS.

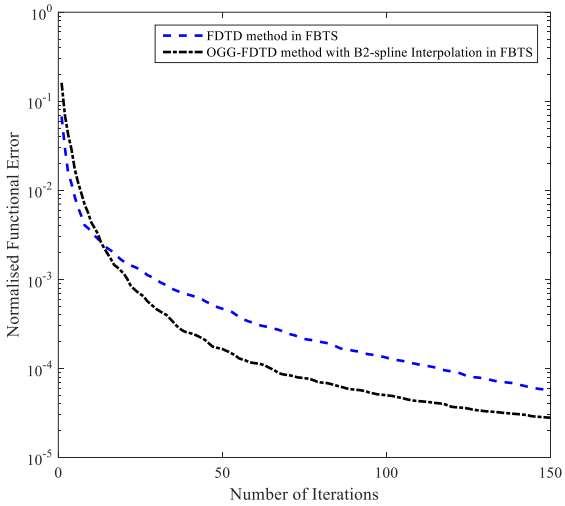


Fig. 9. Normalised functional error versus number of iterations for Case 2.

In this research, the gradient optimization was carried out up to 150 iterations to reconstruct the breast image and minimise the cost functional error. Figure 9 shows that the normalised functional error for OGG-FDTD method with $B_2$-spline interpolation in FBTS is lower as compared to the FDTD method in FBTS. At $150^{th}$ iteration, the difference of normalised functional error between these two methods was $2.87 \times 10^{-5}$. Numerical results demonstrate the efficiency of the proposed method in providing better reconstructed images as compared with the FDTD method in FBTS. Hence, the numerical simulations were able to demonstrate the ability of the proposed method to accurately determine the quantitative information of a heterogeneous realistic breast.

## V. CONCLUSION

In this study, the OGG-FDTD method with $B_2$-spline interpolation in FBTS inverse scattering technique for reconstruction of arbitrary shaped objects embedded in the ROI and the malignant breast tumour detection in heterogeneous dense realistic breast have been presented as Case 1 and Case 2, respectively. The proposed numerical method provides clearer and better reconstructed images as compared with the FDTD method in FBTS. Hence, it can be concluded that the proposed method was able to determine the quantitative information of arbitrary shaped objects and breast composition accurately. The location, shape, size and dielectric properties of a tumour within an arbitrary shape of fibroglandular region also can be determined. For future work, this numerical method can be applied to reconstruct malignant breast tissues in different breast parenchymal density.

## ACKNOWLEDGMENT

This work was supported by *Dana Pelajar Ph.D.* (DPP) Grant F02/DPP/1602/2017, Universiti Malaysia Sarawak (UNIMAS), Ministry of Education Malaysia.

## REFERENCES

[1] E. R. Almeida, J. L. Porsani, I. Catapano, G. Gennarelli, and F. Soldovieri, "GPR data analysis enhanced by microwave tomography for forensic archaeology," *in 15th International Conference on Ground Penetrating Radar (GPR), IEEE*, 2014.

[2] R. Persico, G. Pochanin, V. Ruban, A. Orlenko, I. Catapano, and F. Soldovieri, "Performances of a microwave tomographic algorithm for GPR systems working in differential configuration," *IEEE Journal of Selected Topics in Applied Earth Observations and Remote Sensing*, vol. 9, no. 4, pp. 1343-1356, 2016.

[3] A. Fedeli, M. Pastorino, and A. Randazzo, "A two-step multifrequency imaging technique for ground penetrating radar," *in 10th European Conference on Antennas and Propagation (EuCAP), IEEE*, 2016.

[4] C. Estatico, A. Fedeli, M. Pastorino, and A. Randazzo, "Buried object detection by means of a Lp Banach-space inversion procedure," *Radio Science*, vol. 50, no. 1, pp. 41-51, 2015.

[5] P. M. Ibrahim, K. A. H. Ping, N. S. Wei, Y. Guang, N. Rajaee, and M. Anyi, "Elliptic filter and iterative inversion method for buried object detection applications," *Applied Mechanics and Materials*, vol. 833, p. 164, 2016.

[6] S. A. Shah, Z. Zhang, A. Ren, N. Zhao, X. Yang, W. Zhao, J. Yang, J. Zhao, W. Sun, and Y. Hao, "Buried object sensing considering curved pipeline," *IEEE Antennas and Wireless Propagation Letters*, 2017.

[7] M. Benedetti, M. Donelli, A. Martini, M. Pastorino, A. Rosani, and A. Massa, "An innovative microwave-imaging technique for nondestructive evaluation: Applications to civil structures

monitoring and biological bodies inspection," *IEEE Transactions on Instrumentation and Measurement*, vol. 55, no. 6, pp. 1878-1884, 2006.

[8] S. Kharkovsky and R. Zoughi, "Microwave and millimeter wave nondestructive testing and evaluation-Overview and recent advances," *IEEE Instrumentation & Measurement Magazine*, vol. 10, no. 2, pp. 26-38, 2007.

[9] Y. Deng and X. Liu, "Electromagnetic imaging methods for nondestructive evaluation applications," *Sensors*, vol. 11, no. 12, pp. 11774-11808, 2011.

[10] D. W. Winters, J. D. Shea, P. Kosmas, B. D. Van Veen, and S. C. Hagness, "Three-dimensional microwave breast imaging: Dispersive dielectric properties estimation using patient-specific basis functions," *IEEE Transactions on Medical Imaging*, vol. 28, no. 7, pp. 969-981, 2009.

[11] M. A. Elizabeth, K. A. H. Ping, N. B. Rajaee, and T. Moriyama, "Chebyshev filter applied to an inversion technique for breast tumour detection," *International Journal of Research in Engineering and Technology*, vol. 4, no. 6, pp. 210-218, 2015.

[12] E. Porter, M. Coates, and M. Popović, "An early clinical study of time-domain microwave radar for breast health monitoring," *IEEE Transactions on Biomedical Engineering*, vol. 63, no. 3, pp. 530-539, 2016.

[13] S. Vemulapalli, *Early Breast Cancer Diagnosis Using Microwave Imaging via Space-Frequency Algorithm*, University of Missouri-Kansas City, 2017.

[14] Q. Dong and C. M. Rappaport, "Microwave subsurface imaging using direct finite-difference frequency-domain-based inversion," *IEEE Transactions on Geoscience and Remote Sensing*, vol. 47, no. 11, pp. 3664-3670, 2009.

[15] C. Bardak and M. Saed, "Microwave imaging with a time-reversed finite-difference time-domain technique," *Journal of Electromagnetic Waves and Applications*, vol. 28, no. 12, pp. 1455-1467, 2014.

[16] F. Cakoni, D. Colton, and P. Monk, "Qualitative methods in inverse electromagnetic scattering theory: Inverse scattering for anisotropic media," *IEEE Antennas and Propagation Magazine*, vol. 59, no. 5, pp. 24-33, 2017.

[17] W. Perry, "On the Bojarski-Lewis inverse scattering method," *IEEE Transactions on Antennas and Propagation*, vol. 22, no. 6, pp. 826-829, 1974.

[18] M. Erramshetty and A. Bhattacharya, "Shape reconstruction of dielectric and conducting objects using Linear Sampling Method and limitations," *in 2019 URSI Asia-Pacific Radio Science Conference (AP-RASC), IEEE*, 2019.

[19] I. Rekanos, "Time-domain inverse scattering using Lagrange multipliers: An iterative FDTD-based optimization technique," *Journal of Electromagnetic Waves and Applications*, vol. 17, no. 2, pp. 271-289, 2003.

[20] T. Takenaka, H. Jia, and T. Tanaka, "Microwave imaging of electrical property distributions by a Foward-Backward Time-Stepping method," *Journal of Electromagnetic Waves and Applications*, vol. 14, pp. 1609-1626, 2015.

[21] K. S. Yee, "Numerical solution of initial boundary value problems involving Maxwell's in isotropic media," *IEEE Trans. Antennas Propag.*, vol. 14, no. 3, pp. 302-307, 1966.

[22] J. B. Schneide, *Understanding the Finite-Difference Time-Domain Method*, School of Electrical Engineering and Computer Science, Washington State University, 2016.

[23] R. Nilavalan, I. J. Craddock, and C. J. Railton, "Quantifying numerical dispersion in non-orthogonal FDTD meshes," *IEE Proceedings-Microwaves, Antennas and Propagation*, vol. 149, no. 1, pp. 23-27, 2002.

[24] E. Jiménez-Mejía and J. Herrera-Murcia, "Validation of a non-uniform meshing algorithm for the 3D-FDTD method by means of a two-wire crosstalk experimental set-up," *Ingeniería e Investigación*, vol. 35, pp. 98-103, 2015.

[25] C. Xu, Z. Deng, R. Xiong, and F. Deng, "Time-step program for the sub-cell FDTD modeling of apertures with finite depth," *International Journal of Applied Electromagnetics and Mechanics*, vol. 47, no. 1, pp. 255-262, 2015.

[26] Z. Yang and E. L. Tan, "Stability analyses of non-uniform time-step schemes for ADI- and LOD-FDTD methods," *in Computational Electromagnetics (ICCEM), IEEE International Conference on*, 2017.

[27] M. R. Cabello, L. D. Angulo, J. Alvarez, I. D. Flintoft, S. Bourke, J. F. Dawson, R. G. Martín, and S. G. Garcia, "A hybrid Crank-Nicolson FDTD subgridding boundary condition for lossy thin-layer modelling," *IEEE Transactions on Microwave Theory and Techniques*, vol. 65, no. 5, pp. 1397-1406, 2017.

[28] C. A. De Moura and C. S. Kubrusly, "The Courant-Friedrichs-Lewy (CFL) condition," *Commun. Pure Appl. Math*, vol. 10, no. 2, pp. 363-371, 2013.

[29] B. S. Wee, S. Sahrani, and K. A. H. Ping, "$B_2$-spline interpolation technique for overset grid generation and finite-difference time-domain method," *Progress In Electromagnetics Research C*, vol. 86, pp. 177-190, 2018.

[30] J. Nawawi, S. S Sahrani, K. A. H. Ping, D. A. A. Mat, and D. N. A. Zaidel, "Iterative refinement in inverse scattering technique with median filter," *in 2016 IEEE Asia-Pacific Conference on Applied Electromagnetics (APACE)*, 2016.

[31] E. J. Joseph, K. A. H. Ping, K. Kipli, D. A. A. Mat, S. Sahrani, D. N. A. Zaidel, M. I. Sariphn, and M. H. Marhaban, "Integration of image segmentation method in inverse scattering for brain tumour detection," *Progress In Electromagnetics Research*, vol. 61, pp. 111-122, 2017.

[32] M. Sonnenschein and C. Waldherr, "BI-RADS reporting for breast tomosynthesis (3D-mammography)," *in Atlas of Breast Tomosynthesis, Springer*, pp. 7-57, 2017.

**Bong Siaw Wee** was born in Kuching, Malaysia, in 1982. She received the B.Eng. (Hons) degree in Electronics Engineering from Universiti Teknikal Malaysia Melaka in 2008, and the M.Eng. degree in Electrical Engineering from Universiti Tun Hussein Onn Malaysia in 2012. She is now working towards Ph.D. degree at the Department of Electrical and Electronic Engineering, Universiti Malaysia Sarawak. Her research interests include electromagnetic direct/inverse scattering, optimisation techniques for microwave imaging, and computational electromagnetic.

**Kismet Anak Hong Ping** received the B.Eng. (Hons) degree in Electronics and Telecommunication Engineering from Universiti Malaysia Sarawak, Malaysia, M.Sc. in Digital Communication Systems from Loughborough University, England, and Ph.D. from Nagasaki University, Japan in 1999, 2000, and 2009, respectively.

Currently, he is an Associate Professor at the Department of Electrical and Electronic Engineering, Universiti Malaysia Sarawak. His current research interests focus on electro-magnetic direct/inverse scattering, microwave imaging, optimisation techniques, antenna design, and applications of electromagnetic fields to telecommunications and medicine.

**Shafrida Sahrani** received her B.E. degree in Information Networks, M.E., and Ph.D degrees in Computer Science, from Tokyo University of Technology, Tokyo, Japan in 2005, 2007, and 2013, respectively. She is a Senior Lecturer at the Department of Electrical and Electronic Engineering, Universiti Malaysia Sarawak. Her research interests include computational electromagnetics and microwave imaging.

**Toshifumi Moriyama** was born in Fukui prefecture, Japan, in 1972. He received B.E., M.E., and D.E. degrees in Information Engineering all from Niigata University, Niigata, Japan, in 1994, 1995, and 1998, respectively. In his theses research, he was engaged in radar polarimetry and polarimetric radar sensing of buried objects. He was with Fujitsu System Integration Laboratories Ltd from 1998 to 2003, the National Institute of Information and Communications Technology, Japan (NICT) from 2003 to 2005, and the Earth Observation Research and Application Center (EORC), Japan Aerospace and Exploration Agency (JAXA) in 2006, respectively. He is now an Associate Professor at the Department of Electrical and Electronic Engineering, Nagasaki University, Japan. He is involved in research activities in collaboration with ELEDIA Research Center, and he is the Director of the ELEDIA@UniNAGA. His interests are in inverse scattering, radar polarimetry, microwave remote sensing, and wireless sensor networks.